D/5 N81-14153

INTERACTIONS OF SURFACES WITH THE SOLAR PLASMA *

D. McKeown and C.R. Claysmith
Faraday Laboratories, La Jolla, CA

ABSTRACT

The induced environment is the main source of contamination on a spacecraft. The contamination of surfaces by Volatile Condensable Material (VCM) present on spacecraft is being studied by many investigators both in the laboratory and space. In addition to VCM, the space environment can also be a contributing factor in the contamination of surfaces. We have been investigating the effects of the interaction of the solar plasma with surfaces. Plasma particles impact at energies in the multikilovolt range and penetrate and become trapped in surfaces. Results show that protons can penetrate up to 600 monolayers into surfaces and reach saturation concentrations of 6%.

1.0 INTRODUCTION

Many investigators are conducting fundamental studies both in the laboratory[1,2,3] and space[4,5,6] on VCM contamination of surfaces as a function of temperature. Measurements are being made with the Temperature-Controlled Quartz Crystal Microbalance (TQCM) and include qualitative analysis of contaminant species, adsorption and desorption rates, sticking coefficients and changes in optical properties of surfaces. The TQCM[7] was developed in 1973 by Faraday Laboratories for NASA to monitor contamination between -60 and +100°C in space chambers. Recently, we completed construction of an extended temperature range TQCM system for space flight having higher mass sensitivity and ground command of temperature. Operating temperatures are attained either with radiative coolers or thermoelectric devices. The Air Force Materials Laboratory has a radiatively-cooled TQCM in flight on SCATHA[8] that was launched on January 30, 1979. JPL has a thermoelectrically controlled system ready for flight on a NOAA operational environmental satellite[9]. MSFC has both radiatively and thermoelectrically controlled systems awaiting flight on Shuttle[10]. The SCATHA system is shown in Fig. 1. It consists of a controller and two radiatively cooled sensor heads. The sensors are high mass sensitive 15-MHz optically-polished quartz crystals plated with aluminum.

The Principal Investigator for the SCATHA experiment is D.F. Hall. He has reported important data[4] on the measurement of surface contamination enhanced by spacecraft charging in the multikilovolt range[11]. In the

* Supported in part by ONR Contract N00014-78-C-0373.
For presentation at the 11th Space Simulation Conference, Johnson Space Center, Houston, TX, 23-24 Sept. 1980.

experiment, one TQCM views space. The other periodically views space and the sun at 1 rpm. Data from the sun viewing TQCM is significantly different from the TQCM pointed into space. The mass accumulation rate of the sun viewing TQCM is relatively insensitive to sensor temperatures betweer -34 and +58°C. The space viewing TQCM temperature showed mass accumulation only for temperatures below -30°C and mass desorption at higher temperatures. The most probable reason for the difference is solar UV radiation modifying the contamination and increasing its desorption energy[4]. Another effect that is independent of temperature and results in mass accumulation is the penetration and trapping of solar plasma into the aluminum surface plated onto the TQCM. We have been investigating in the laboratory the effects impacts of protons and alpha particles present in the solar plasma have on surfaces.

2.0 LABORATORY MEASUREMENTS

A photograph of the plasma generator used for the measurements is shown in Fig. 2. A plasma is generated by first creating a narrow-energy ion beam. Gas is fed into a flat cylindrical chamber with circular apertures on the axis. Electrons from a filament are made to spiral along this axis by an axially directed magnetic field generated by a solenoid. The spiraling electrons collide with the neutral atoms to produce ionization. The ions are extracted from the chamber (anode), pass through the focusing system, a series of metal tubes separated with ceramic insulators, and accelerate towards the target (cathode). The target is an aluminum plated 20 MHz quartz crystal for measuring mass gain or loss during bombardment. A 20 MHz crystal was used because of its high-mass sensitivity of 8.78×10^{-10} g/cm^{2}Hz needed to facilitate the measurements. The ion impact energy is controlled by varying the target potential.

Beam fluxes of about 10^{14} ions per second per cm^2 are easily obtained with any gas using this beam generator. In our experiments, only noble gas atoms were chosen as bombarding ions for the following reasons. Monatomic beams of singly charged ions of noble gases can readily be formed without mass analysis. They are available in pure quantities. The range of atomic number and weight of these gases is more than adequate for these investigations. They are inert so that reactions with surfaces are minimized. The generator is operated in a VacIon pumped chamber.

The effects of bombarding Al with 0.35 mA He^+ at 2.5 keV is shown in Fig. 3. During the first 35 min of impact the target increases in mass because the mass of He^+ trapped in the surface was greater than the mass of Al eroded by sputtering. For the next 15 min, the mass gained and lost is about equal, and the net mass change is approximately zero. After 50 min, the target became saturated with He. The mass loss rate is then equal to the sputtering yield of aluminum in He^+.

3.0 ION-SURFACE INTERACTIONS

3.1 Surface Mass Loading

The penetration and trapping of ions in a solid surface shown in Fig. 3 can be described by the mass rate of change per unit area,

dM/dt, of a target under bombardment.

$$dM/dt = \alpha m_1 i - \beta(t) m_1 - \mu m_2 i \qquad (1)$$

The absorption coefficient, α, is the fraction of incident particles that penetrate and become trapped in the target. The beam flux is i in ions/cm^2-s. The mass of the bombarding ion and of a target atom are, respectively, m_1 and m_2. The re-emission coefficient, $\beta(t)$ is the number of trapped particles re-emitted as succeeding layers of target atoms are sputtered. The sputtering yield, μ, is the number of target atoms ejected per incident ion. At $t = 0$, $\beta(t) = 0$, and as t becomes large, $\beta(t) \rightarrow \alpha i$. Once $\beta(t) = \alpha i$, the target will lose mass at a constant rate due to sputtering.

3.2 Ion Penetration into Surfaces

To penetrate beyond the first layer of atoms of a solid the inequality

$$\sigma n^{2/3} \geq 1 \qquad (2)$$

must hold, otherwise the particle will probably be reflected. The atomic number density of the solid is n, and $n^{2/3}$ represents the area number density seen by the incident particle with a total binary cross section, σ. This inequality is satisfied for protons and alpha particles in the solar plasma.

Although the cross sections at these low energies are not known accurately, Bohr[12] has shown a reasonable cross section to be

$$\sigma \approx \frac{2\pi a_o^2 E_R}{2.72} \frac{Z_1 Z_2}{(Z_1^{2/3} + Z_2^{2/3})^{1/2}} \frac{m_1 + m_2}{m_2} \frac{1}{E_1} \qquad (3)$$

which is replaced by

$$\sigma = \pi R^2 \qquad (4)$$

whenever $\sigma \gg \pi a_o^2/(Z_1^{2/3} + Z_2^{2/3})$. At the lowest energies the binary collision cross section approaches the gas kinetic value. R is the distance of closest approach obtained as the solution of

$$R\, m_2 E/(m_1 + m_2) = 2 Z_1 Z_2 E_R a_o \exp\left[-R(Z_1^{2/3} + Z_2^{2/3})^{1/2}/a_o\right] \qquad (5)$$

Subscripts 1 and 2 designate incident and target particles, respectively, with E the kinetic energy, m the mass, Z the atomic number, a_o the Bohr radius and E_R the Tydberg energy.

To obtain the distribution of the penetrating ions it is necessary to consider their motion in the solid. Although the ions are probably neutralized upon entering the solid this is expected to be of no consequency since hard sphere type collisions are assumed to occur. For protons and alpha particles, $m_2/m_1 > 1$, large angle scattering occurs at each collision giving an erratic rectilinear path which resembles a diffusion process. In fact, the slowing down process is treated like that of neutrons where the particle slowing down density for a plane flux i is

$$q = \frac{i}{(4\pi R)^{1/2}} e^{\frac{-x^2}{4R}} \tag{6}$$

where R is the "Fermi age." The density q represents the number of particles per cm^3 per second that slow down past an energy F at a given depth x in the solid. If $m_2/m_1 > 1$ the angular deflection of the incident particle from its direction of travel is small and the particle straggles about the penetration depth with an approximate Gaussian distribution.

Because the notion of range is complex, it is customary to define a linear, a vector and a projected range. The linear range is the total rectilinear path traversed by the particle to the point of stopping while the vector range is the vector distance from point of entry into the solid to the end point. Projection of the vector distance along a line normal to the surface gives the projected range. An approximate relation between the average linear range $[R_L]$ and the average projected range $[R_p]$ (or mean range) was developed by Linhard and Scharff[13] as

$$[R_L] \approx [R_p] \left(1 + \frac{1}{3}\frac{m_2}{m_1}\right) \tag{7}$$

for an inverse square potential. For $m_2/m_1 \leq 1$, approximation (7) is quite accurate but, for $m_2/m_1 > 1$ the approximation has application to a portion of the low energy region only.

Scattering near the end point of the particle travel is probably a many-body collision problem and not the binary one assumed to obtain the distributions discussed in the previous section. If relation (2) is used as a necessary criterion for halting the motion of the incident particle, the cross section must be about the gas kinetic value,

$\sigma \approx 5 \times 10^{-16} cm^2$; cross sections of these magnitudes correspond to energies the de Brolie wave length is comparable to the lattice separation indicating that more than one target atom contributes to a collision.

Andersen and Sigmund[14] have presented a model for non-binary scattering which is of importance at much higher energies than indicated by (2). It recognized the fact that, with such small mean free paths, correlations between successive collisions cannot be neglected in the low energy region. The model assumed involves a set of crystal lattice rows which are resolved into stacked symmetric rings of atoms. The incident particle moves along the symmetry axis of these rings with the projectile-ring interaction as the basic event with the ring presenting an effective potential field to the incident atom.

If the incident particle is aligned along the symmetry axis, close collisions become improbable because the field keeps the particle near the symmetry axis to produce channeling. For the interpretation of penetration distributions known in the literature as "supertails" it is important to investigate the low energy collisions to determine the density of vacancies, interstitials and self-interstitials created. From this, estimates of further projectile penetration by diffusion after the slowing down process can be made. Using a Born-Mayer potential for each lattice atom, a new reflecting (or stopping) energy replaces the one determined through (2) and is found to be

$$R_{refl} \approx p\, A e^{-L/a} \qquad (8)$$

whenever $m_1 \gg m_2$. Constants p and L define the number of particles in the ring and radious of the ring element; A and a are the potential parameters. Reflection energies given by (8) are somewhat higher than that found through (2); for alpha particles in heavy materials, typical estimates are 5-10 eV.

3.3 Diffusion of Trapped Particles

Channeling explains the penetration to ranges of a few microns for particles in the keV range but "supertails" extend to depths of several microns. A possible explanation to these deep penetrations is the steady state diffusion approach of Sparks[15]. He assumes the diffusion of vacancies and self-interstitials created by the incident particles is unaffected by the relatively small number of implanted ions. With the bombarding particles forming substitutionals through the annihilation of vacancies two general forms of the integral penetration distributions, $n_s(x)$, result which may be expressed as

$$n_s(x) \approx \exp[-k(x-1)] \; ; \; x > 1 \qquad (9)$$

and

$$n_s(x) \approx \frac{d^{2+r}}{(x - l + d)^{2+r}} \; ; \; x > l \; . \qquad (10)$$

The constant d depends upon the vacancy density interstitial density and the diffusion coefficient; l is located approximately at the edge of the stopping region. Distribution (10) normally occurs if vacancies and self-interstitials are created and annihilated in pairs. For distribution (9) to obtain the vacancies, the self-interstitials must be created at different rates which means that most of the interstitials must be of the bombarding particle type.

4.0 ION-BOMBARDMENT OF ALUMINUM

Laboratory measurements were made on aluminum to determine the effect the ions present in the solar plasma have on low atomic weight surfaces. The main constituents of the plasma are proton and alpha particles[16] having energies in the multikilovolt range. Heavier ions, such as iron, were not considered because their densities are too low to produce measurable effects.

Once the protons penetrate the surface, little will diffuse out because of the affinity of aluminum for hydrogen[17]. Any alpha particles that penetrate the surface will readily diffuse out because of the inert nature of helium. The principle effect of alpha impacts will be that of sputtering the surface.

To determine the saturation concentration of protons for aluminum, the distribution function q given by (6) can be used. The distribution is for the case $m_1 > m_2$. It has a maximum near the surface because of large angle scattering that occurs for the case in which the incident particle mass m_1 is less than the target atom mass m_2.

The mean penetration depth $[R_p]$ of the particles needed to scale the distribution function can be found from the $\rho - \epsilon$ relationship of Lindhard and Scharff,[18] which relates the range-energy of particles in solids:

$$\rho = R_m\left(1 - \frac{A_2}{3A_1}\right) \frac{166}{(Z_1^{2/3} + Z_2^{2/3})} \frac{A_1}{(A_1 + A_2)^2} \qquad (11)$$

$$\epsilon = \frac{33}{Z_1 Z_2 (Z_1^{2/3} + Z_2^{2/3})^{1/2}} \frac{A_2}{A_1 + A_2} E_1 \qquad (12)$$

where the subscripts 1 and 2 refer to the incident ion and the target atom, and E_1 is the energy of impact in keV.

Davie's group has shown that the ρ - ϵ relationship is accurate to about 20% for $\epsilon < 10$. Values for ρ, knowing ϵ, have been plotted by them for $0 < \epsilon < 10$ and $0 < \rho < 100$.[19]

The absorption coefficient α was found, experimentally, to be about 0.01.

The velocity ν at which the surface is sputtered was calculated using a yield, for Al in He^+ is the same as that for He^{++} (alpha particles). Experimentally, the yield for He^+ at 8 keV was found to be 0.3. The average erosion velocity of Al using these yields for He^+ and He^{++} is $\nu \approx 10^{-8}$cm/hr. By assuming that diffusion is zero, the saturation concentration of trapped hydrogen in aluminum was found.

The saturation distribution of hydrogen in aluminum, in hydrogen atoms per aluminum atom N_H/N_{Al}, is shown in Fig. 4.

5.0 CONCLUSIONS

A spacecraft traveling beyond the magnetosphere passes into the tenuous upper atmosphere of the sun known as the solar plasma. The plasma is composed mainly of electrons, protons, and alpha particles. Protons and alpha particles will impact at energies ranging up to 10 keV during periods of a quiet run and approximately 20 keV during solar activity.[16]

Low atomic weight metal surfaces will be damaged by the penetration and trapping of protons. Surface properties would be affected by the formation of hydrides in concentrations approaching 6%. It will take several years before surface properties would be significantly affected because of the low density of protons in the solar plasma. Damage would be accelerated during solar activity and for spacecraft passing near the sun.

Effects on nonconducting materials such as plastics, which are composed of large amounts of hydrogen, will be more pronounced because most of the plasma will be absorbed. For these materials, changes would become apparent in a few years. The protons and alpha particles that penetrated these surfaces will displace surface atoms. It takes about 25 eV to displace an atom from its lattice point[20]. In a year the plasma will produce about 10^{17} atomic displacements. In surface coatings, the displacements will produce discoloration through the creation of color centers and effect the solar absorptance.

6.0 REFERENCES

1. Muscari, J.A., and Jacobs, S., "Silver-Teflon Contamination UV Radiation Study", Proceedings USAF/NASA International Spacecraft Contamination Conference, AFML-TR-78-190, NASA-CD-2039 (1978) pp. 1112 - 1127.

2. Richmond, R.G. and Kelso, R.M., Effectiveness of Shuttle Orbiter Payload Bay Liner as a Barrier to Molecular Contamination from Hydraulic Fluids", Proceedings USAF/NASA International Spacecraft Contamination Conference, AFML-TR-78-190, NASA-CD-2039 (1978) pp. 846 - 862.

3. Visentine, J.T., Richmond, R.G., and Kelso, R.M., "Experiment to Measure Molecular Outgassing Rates from Shuttle Orbiter Flexible Reusable Surface Insulation (FRSI)", Progress in Astronautics and Aeronautics, Vol. 56, AIAA (1977) pp. 197 - 213.

4. Hall, D.F., "Flight Experiment to Measure Contamination Enhancement by Spacecraft Charging", Proceedings SPIE Conference, North Hollywood, CA (1980) Vol. 216 - 15.

5. Miller, F.R., "Shuttle Induced Environment Contamination Monitor", Proceedings USAF/NASA International Spacecraft Contamination Conference, AFML-TR-78-190, NASA-CD-2039 (1978) pp. 534 - 566.

6. Lynch, J.T., "Quartz Crystal Microbalance (QCM) Monitor of Contamination for LES-8/9", 9th Space Simulation Conference, NASA CP-2007 (1977) pp. 211 - 219.

7. McKeown, D., Corbin, W.E. Jr. and Naumann, R.J., "Thermoelectrically Cooled Quartz Crystal Microbalance", 7th Conference on Space Simulation, NASA SP-336 (1973) pp. 345 - 358.

8. McKeown, D., Claysmith, C.R., Breckenridge, W.T. Jr., Dummer, R.S., "Temperature Controlled Quartz Crystal Microbalance System", Report AFML-TR-77-83, AFML/MBE, Wright-Patterson AFB, OH (1977).

9. Maag, C.R.,"NOAA-B Contamination Monitoring Instrumentation", Proceedings SPIE Conference, North Hollywood, CA (1980) Vol. 216 - 15.

10. McKeown, D. and Claysmith, C.R., "Quartz Crystal Microbalance Systems for Shuttle Contamination Measurements", Proceedings USAF/NASA International Spacecraft Contamination Conference, AFML-TR-78-190, NASA-CD-2039 (1978) pp. 605 - 629.

11. Kuch, G.A. and Holaday, B.H., "A Description of the Space Test Program P78-2 Spacecraft and Payloads" Report SAMSO TR-78-24 (1978).

12. Bohr, N., Penetration of Atomic Particles Through Matter, Det. Kgl. Dan. Vidensk, Selsk., Mat. - Frs. Medd., (1948).

13. Linhard, J., Scharff, M., and Schiott, H.E., Range Concepts and Heavy Ion Ranges, Dt. Kgl. Dan. Vidensk. Selsk., Mat. - Fys. Medd., Vol. 33, No. 14 (1963), pp. 643 - 721.

14. Andersen, H.H., and Sigmund, P., "Simple Non-Binary Scattering Model Applicable to Atomic Collisions and Crystals at Low Energies", Dt. Kgl. Dan. Vidensk. Selsk., Mat. - Fys. Medd., Vol. 4 (1966), pp. 723 - 752.

15. Sparks, M., "Theory of Supertails of Ions Bombarded into Crystals", Phys. Rev. Letters, Vol. 17, (1966), pp. 1247 - 1249.

16. Freeman, J.W., Van Allen, J.A., and Cahil, L.J., "Explorer 12 Observations of the Magnetospheric Boundary and the Associated Solar Plasma on Sept. 13, 1961", Beophys. Res., 68, (1963), pp. 2121 - 2130.

17. Bergstrom, I., Brown, F., Davies, J.A., Geiger, J.S., Graham, R.L., and Kelly, R., "On the Electromagnetic Separation Method of Preparing Radioactive Sources for Precision β - Spectroscopy", Nucl. Instr. Methods, 21, 249 (1963), pp. 249 - 261.

18. Lindhard, J., and Scharff, "Energy Dissipation by Ions in the keV Region", Phys. Rev., 124 (1961), pp. 124 - 132.

19. Davies, J.A., McIntyre, J.D., and Sims, G., "The Range of C^{137} Ions of keV Energies in Germanium", Can. Jour. Chem., 40, (1962), pp. 1605 - 1621.

20. Seitz, F., and Koehler, J.S., "Displacement of Atoms During Irradiation", Solid State Physics, (Academic Press, New York, 1956), pp. 307 - 448.

Fig. 1 SCATHA TQCM System without RPA Installed

Fig. 2 Plasma Generator

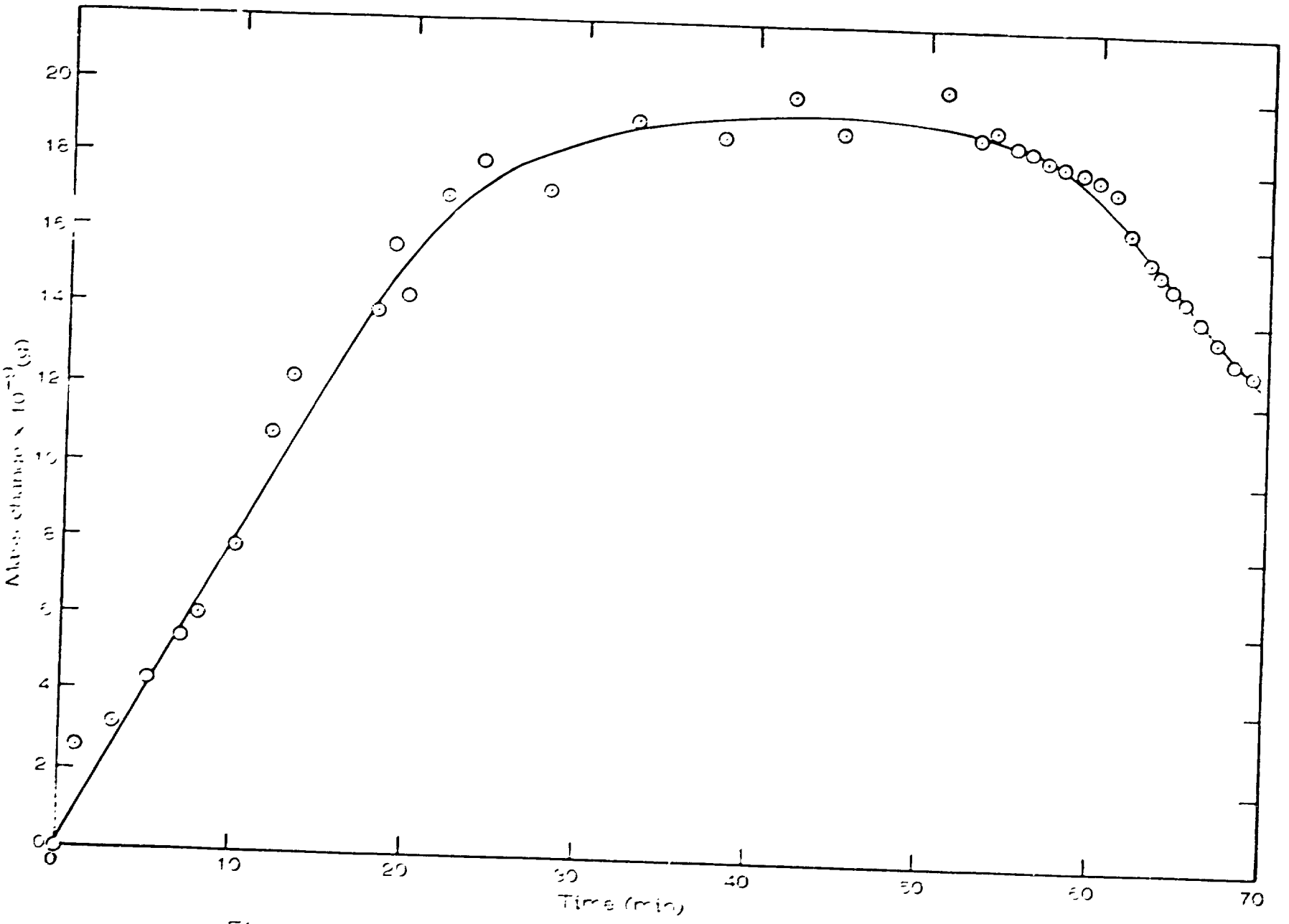

Fig. 3 Mass change of Al target under He⁺ bombardment at 2.5 keV

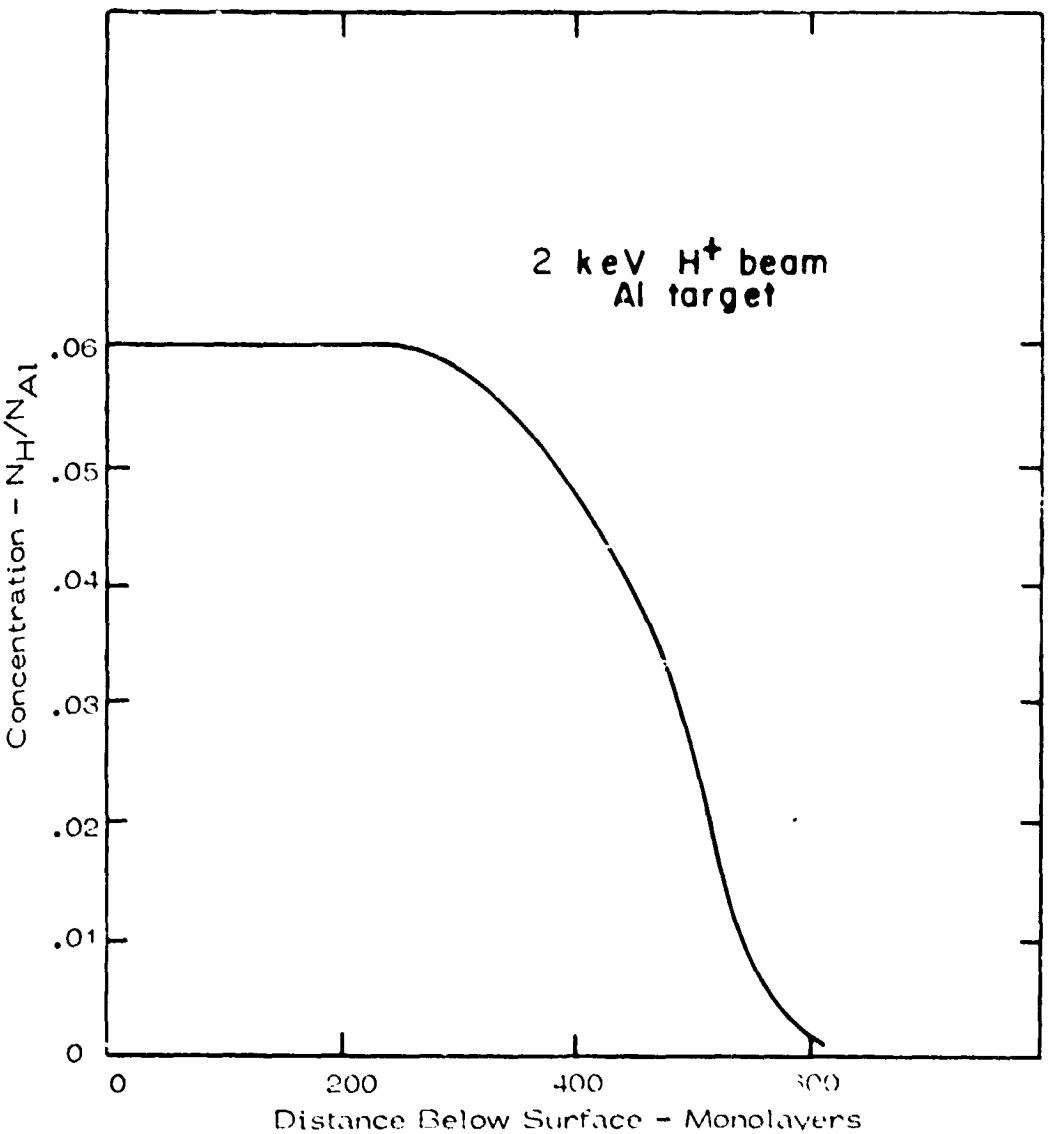

Fig. 4 Saturation concentration of hydrogen in aluminum